

# Superconductivity and phonon self-energy effects in $\text{Fe}_{1+y}\text{Te}_{0.6}\text{Se}_{0.4}$

S.-F. Wu,<sup>1,\*</sup> A. Almoalem,<sup>2</sup> I. Feldman,<sup>2</sup> A. Lee,<sup>1</sup> A. Kanigel,<sup>2</sup> and G. Blumberg<sup>1,3,†</sup>

<sup>1</sup>*Department of Physics and Astronomy, Rutgers University, Piscataway, NJ 08854, USA*

<sup>2</sup>*Physics Department, Technion-Israel Institute of Technology, Haifa 32000, Israel*

<sup>3</sup>*National Institute of Chemical Physics and Biophysics, 12618 Tallinn, Estonia*

(Dated: March 3, 2022)

We study  $\text{Fe}_{1+y}\text{Te}_{0.6}\text{Se}_{0.4}$  multi-band superconductor with  $T_c = 14$  K by polarization-resolved Raman spectroscopy. Deep in the superconducting state, we detect pair-breaking excitation at  $45\text{ cm}^{-1}$  ( $2\Delta = 5.6\text{ meV}$ ) in the  $XY(B_{2g})$  scattering geometry, consistent with twice of the superconducting gap energy (3 meV) revealed by ARPES on the hole-like Fermi pocket with  $d_{xz}/d_{yz}$  character. We analyze the superconductivity induced phonon self-energy effects for the  $B_{1g}(\text{Fe})$  phonon and estimate the electron-phonon coupling constant  $\lambda^\Gamma \approx 0.026$ , which is insufficient to explain superconductivity with  $T_c = 14$  K.

**Introduction** – Since the discovery of the multi-band iron-based superconductors (FeSCs) in 2008 [1], a unified understanding the pairing mechanism in FeSCs remains in a focus of attention [2–8]. One step towards understanding the pairing mechanism is to study the superconducting (SC) gaps on different pockets of the Fermi surface (FS) [5, 9].

The chalcogenide family  $\text{Fe}_{1+y}\text{Te}_{1-x}\text{Se}_x$  has simple stoichiometry and crystal structure which can be viewed as stacks of  $\text{FeTe}_{1-x}\text{Se}_x$  layers [Fig. 1(a)]. Superconductivity in this system was first found at 8 K in the non-magnetic FeSe. With about 60% isovalent substitution of Se for Te,  $T_c$  in  $\text{Fe}_{1+y}\text{Te}_{0.6}\text{Se}_{0.4}$  increases to 14 K [10]. Thus, the non-magnetic and tetragonal  $\text{Fe}_{1+y}\text{Te}_{0.6}\text{Se}_{0.4}$  is an ideal system to study the SC order parameter, without the effect of coexisting or interacting with other electronic orders.

Polarization-resolved Raman spectroscopy has been used to study the pair-breaking excitations in different symmetry channels [12–18] and for estimation of the electron-phonon coupling [19–21] in FeSCs. Previous Raman studies on  $\text{Fe}_{1+y}\text{Te}_{1-x}\text{Se}_x$  were focused on the lattice dynamics [22–25] and the magnetic excitations [25], while the superconducting features for  $\text{Fe}_{1+y}\text{Te}_{0.6}\text{Se}_{0.4}$  have not been well established.

In this work, we use polarization-resolved Raman spectroscopy to study the pair breaking excitations in  $\text{Fe}_{1+y}\text{Te}_{0.6}\text{Se}_{0.4}$ . In the SC state, we identify the coherence peak at  $45\text{ cm}^{-1}$  ( $2\Delta = 5.6\text{ meV}$ ) in the  $XY(B_{2g})$  in  $D_{4h}$  scattering geometry with cross-polarized light along Fe-Te/Se directions. The peak energy is close to the twice of the gap energy (3 meV) on the hole-like FS pocket with  $d_{xz}/d_{yz}$  character around  $\Gamma$  point, as determined by ARPES. We investigate the superconductivity induced phonon self-energy effects for the  $B_{1g}(\text{Fe})$  phonon mode and estimate the electron-phonon coupling constant  $\lambda^\Gamma \approx 0.026$ , which is very weak to explain  $T_c = 14$  K in  $\text{Fe}_{1+y}\text{Te}_{0.6}\text{Se}_{0.4}$ .

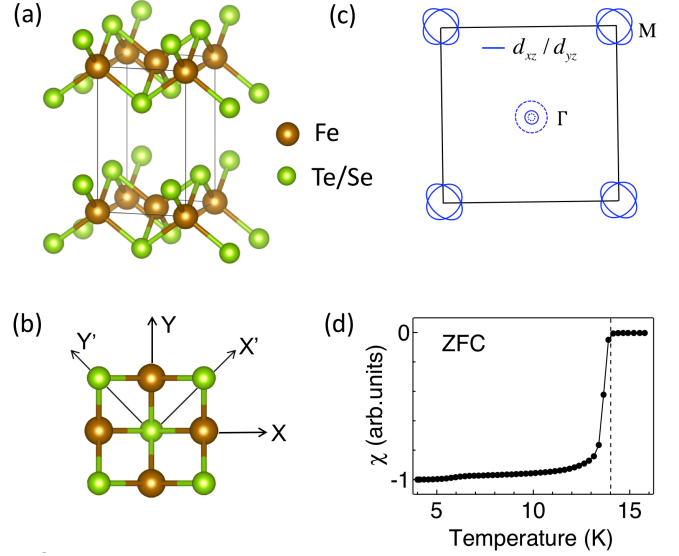


FIG. 1. (a) Crystal structure of  $\text{Fe}_{1+y}\text{Te}_{0.6}\text{Se}_{0.4}$ . (b) Definition of  $X$ ,  $Y$ ,  $X'$  and  $Y'$  directions in a 2-Fe unit cell. (c) Schematic representation of Fermi surfaces of  $\text{Fe}_{1+y}\text{Te}_{0.6}\text{Se}_{0.4}$  in the 2-Fe Brillouin zone (BZ) [11]. (d) "Zero-field-cool" magnetic susceptibility measured with magnetic field  $H=4$  Oe along the  $c$ -axis direction.

**Experimental** – The single crystals of  $\text{Fe}_{1+y}\text{Te}_{0.6}\text{Se}_{0.4}$  were grown using modified Bridgman method [26]. The composition of  $\text{Fe}_{1+y}\text{Te}_{0.6}\text{Se}_{0.4}$  was determined on samples from the same growth batch by energy-dispersive x-ray (EDX) analysis. The nominal composition of excess Fe ( $y$ ) in  $\text{Fe}_{1+y}\text{Te}_{0.6}\text{Se}_{0.4}$  is about 2%, while the real value of  $y$  is close to zero [26]. The magnetic susceptibility confirming a sharp SC transition at  $T_c=14$  K is shown in Fig. 1(d).

The  $\text{Fe}_{1+y}\text{Te}_{0.6}\text{Se}_{0.4}$  single crystals used for Raman measurements were cleaved in nitrogen gas atmosphere in a glove bag, then immediately loaded into connected continuous helium flow optical cryostat and quickly cooled down to 250 K within 5 minutes to avoid surface contamination. All the Raman scattering measurements

\* sw666@physics.rutgers.edu

† girsh@physics.rutgers.edu

were performed using the  $\text{Kr}^+$  laser line at 647.1 nm (1.92 eV) in a quasi-back scattering geometry along the crystallographic  $c$ -axis with an instrumental resolution about  $1.5 \text{ cm}^{-1}$ . The excitation laser beam was focused into a  $50 \times 100 \text{ }\mu\text{m}^2$  spot on the  $ab$ -surface, with the incident power around 10 mW and 2 mW for normal state and superconducting state measurements, respectively. The scattered light was collected and analyzed by a triple-stage aberration corrected Raman spectrometer and recorded using a liquid nitrogen-cooled charge-coupled detector. The Raman spectra were corrected for the spectra response of the spectrometer and the detector. The temperature shown in this paper has been corrected for laser heating. An empirical heating coefficient  $1 \text{ K/mW}$  was applied according to FeSe [14, 27, 28].

In this manuscript, we define the  $X$  and  $Y$  directions along the two-Fe unit cell basis vectors (at  $45^\circ$  degrees from the Fe-Fe directions) in the tetragonal phase, whereas  $X'$  and  $Y'$  are along the Fe-Fe directions [Fig. 1(b)]. Raman spectra were recorded for  $(\hat{e}_i \hat{e}_s) = (XX)$ ,  $(XY)$ ,  $(X'X')$  and  $(X'Y')$  polarization geometries in the  $ab$ -plane, where  $\hat{e}_i$  and  $\hat{e}_s$  represent the incident and scattered light polarization, respectively.

For crystals with point group symmetry  $D_{4h}$ , the  $XX$ ,  $X'Y'$  and  $XY$  geometries probe  $A_{1g}+B_{1g}$ ,  $A_{2g}+B_{1g}$  and  $A_{2g}+B_{2g}$  channels, respectively [29]. Assuming the  $A_{2g}$  response is negligible [12] and using the background estimated from the  $X'Y'$ -symmetry electronic continuum [18, 30], the Raman response in  $(\mu\nu)$  scattering geometry  $\chi''_{\mu\nu}(\omega, T)$  can be obtained:  $\chi''_{\mu\nu}(\omega, T) = I_{\mu\nu}(\omega, T)/[1+n(\omega, T)]$ , where  $I_{\mu\nu}(\omega, T)$  is the Raman intensity after background subtraction and  $n(\omega, T)$  is the Bose-Einstein factor.

*The normal state* – The  $\text{Fe}_{1+y}\text{Te}_{0.6}\text{Se}_{0.4}$  crystal structure belongs to the space group  $P4/nmm$  (point group  $D_{4h}$ ). The  $\Gamma$  point Raman active modes are  $\Gamma_{\text{Raman}} = A_{1g} + B_{1g} + 2E_g$ . The  $A_{1g}$  and  $B_{1g}$  modes are related with Te/Se and Fe atoms  $c$ -axis lattice vibrations, respectively.

In Fig. 2, we show the normal state Raman spectra for four in-plane scattering geometries at 25 K. The observed mode at around  $162 \text{ cm}^{-1}$  and the mode at around  $207 \text{ cm}^{-1}$  in  $XX$  scattering geometry are assigned to  $A_{1g}(\text{Te/Se})$  and  $B_{1g}(\text{Fe})$  modes, respectively [24, 25]. The comparison of the phonon frequencies and line-widths obtained in this work with previous studies [24, 25] are summarized in Table I. The phonon frequency for

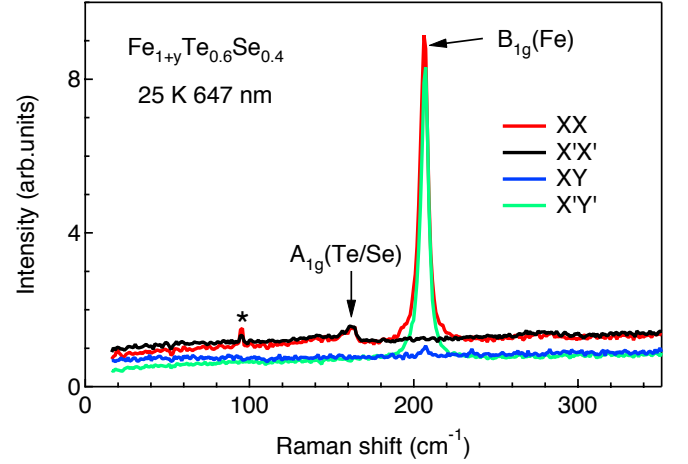


FIG. 2. Raman intensity of  $\text{Fe}_{1+y}\text{Te}_{0.6}\text{Se}_{0.4}$  at 25 K for  $XX$ ,  $XY$ ,  $X'X'$  and  $X'Y'$  scattering geometries. The star represents a laser plasma line.

both modes and the line-width for the  $B_{1g}(\text{Fe})$  mode are consistent with Ref. [24, 25]. In contrast, the line-width for the  $A_{1g}(\text{Te/Se})$  mode in this work is about 3~4 times sharper than in Ref. [24, 25]. We note that the spectra shown in Fig. 2 lack the two features reported in Ref. [25]: the low frequency bump/tail appearing in all in-plane scattering geometries and a substantial ‘leakage’ intensity of  $A_{1g}$  phonon into cross scattering geometries. The absence of these two features indicates the quality of cleaved surface in this study.

*The superconducting state* – Before looking into the Raman features observed in the SC state for  $\text{Fe}_{1+y}\text{Te}_{0.6}\text{Se}_{0.4}$ , we recall the SC gap values obtained by complementary spectroscopic probes. Angle-resolved photoemission spectroscopy (ARPES) revealed nodeless SC gaps with small or negligible in-plane anisotropy on both hole-like and electron-like FS pockets [26, 32, 33]. In addition to the SC gap of 1.8 meV for the topological surface state around the  $\Gamma$  point [33], two close to isotropic gap values for bulk bands with  $d_{xz}/d_{yz}$  character were reported: a 3 meV gap for the hole-like FS pocket centered around the  $\Gamma$  point [26] and a larger, about 4.2 meV gap for the electron pocket around the M point [32]. The scanning tunneling spectroscopy (STS) showed SC coherence peaks at 1.5 meV and a shoulder at 2.5 meV [34]. The infrared spectroscopy (IR) revealed two SC gaps at 2.47 meV and 5.08 meV [35]. The measurements of specific heat confirmed the nodeless nature of the SC order parameter with an averaged gap value 2.3 meV [36]. At the energy scale of the sum of SC gaps on the hole-like and electron pockets with  $d_{xz}/d_{yz}$  character, a 6.5 meV neutron-spin-resonance mode was reported below  $T_c$  at  $\mathbf{Q} = (\pi, \pi)$  [2-Fe BZ] by inelastic neutron scattering (INS) measurements [37]. The values of the SC gaps and bosonic modes deduced from different spectroscopies are summarized in Table II.

TABLE I. Comparison of the phonon frequencies ( $\omega$ ) and the line-widths ( $\gamma$ ) for  $A_{1g}(\text{Te/Se})$  and  $B_{1g}(\text{Fe})$  modes for  $\text{Fe}_{1+y}\text{Te}_{1-x}\text{Se}_x$  with similar compositions at 5 K. Units are in  $\text{cm}^{-1}$ .

Sample	$\omega_{A_{1g}}$	$\gamma_{A_{1g}}$	$\omega_{B_{1g}}$	$\gamma_{B_{1g}}$
$\text{FeTe}_{0.6}\text{Se}_{0.4}$ [25]	162.6	27.2 [31]	207.7	8.8 [31]
$\text{Fe}_{0.95}\text{Te}_{0.56}\text{Se}_{0.44}$ [24]	162	20	207	5
$\text{Fe}_{1+y}\text{Te}_{0.6}\text{Se}_{0.4}$ (this work)	162	6.9	208.2	4

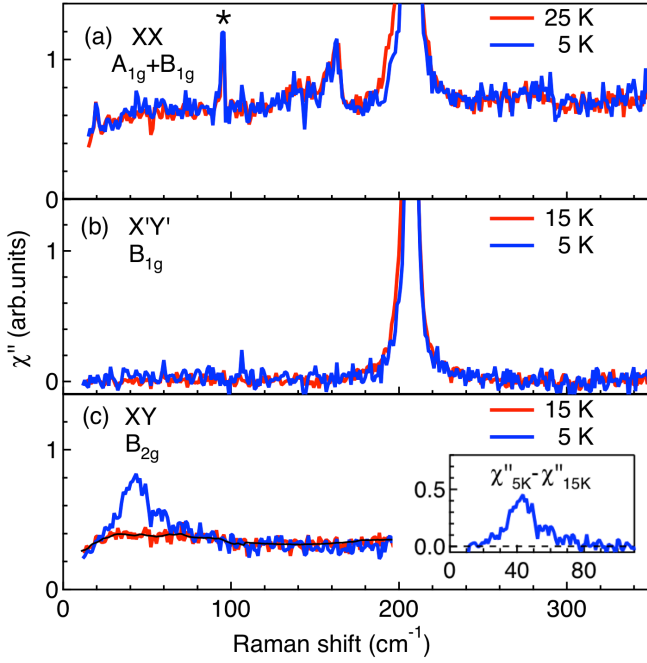


FIG. 3. Raman response of  $\text{Fe}_{1+y}\text{Te}_{0.6}\text{Se}_{0.4}$  above and below  $T_c$  in  $XX$  (a),  $X'Y'$  (b) and  $XY$  (c) scattering geometries. The star in (a) indicates a laser plasma line. The solid black line in (c) represent the smoothed curve for the Raman response at 15 K which is used to calculate the difference between the response above and below  $T_c$  in  $XY$  scattering geometry shown in the inset of (c).

In Fig. 3, we present the Raman response above and below  $T_c$  for three scattering geometries. For the  $XX$  and  $X'Y'$  scattering geometries, the electronic continuum barely changes upon cooling below  $T_c$ . In contrast, for  $XY$  scattering geometry a clear peak at around  $45 \text{ cm}^{-1}$ , which we relate to the pair-breaking excitation, emerges below  $T_c$ . Since the peak's energy is about  $5.6 \text{ meV}$ , based on the Table II, we assign it to the gap  $2\Delta_2$  on the hole-like FS pocket with the  $d_{xz}/d_{yz}$  character [39] around  $\Gamma$  point with a typical gap value  $\Delta_2 = 3 \text{ meV}$ .

TABLE II. The summary of the values for SC gaps and bosonic modes deducted from ARPES, STS, IR, Specific heat, Raman scattering, and INS measurements for  $\text{Fe}_{1+y}\text{Te}_{0.6}\text{Se}_{0.4}$  with similar compositions.  $\Delta_1$ ,  $\Delta_2$  and  $\Delta_3$  represent three energy scales of gap values.  $E_{CM}$  represents the energy of the bosonic mode. All energies are given in units of meV.

	$\Delta_1$	$\Delta_2$	$\Delta_3$	$E_{CM}$
ARPES	1.8 [33]	3 [26]	4.2 [32]	
STS	1.5 [34, 38]	2.5 [34]		
IR		2.47 [35]	5.08 [35]	
Specific heat		2.3 [36]		
Raman		2.8 (this work)		
INS				6.5 [37]

from the ARPES measurement [26]. The pair-breaking peak associated with the larger gap  $2\Delta_3 = 8.4 \text{ meV}$  on the electron pockets around  $M$  point is not detected in the  $B_{2g}$  channel. In contrast, in optimally-doped  $\text{Ba}(\text{Fe}_{0.939}\text{Co}_{0.061})_2\text{As}_2$ , a similar single peak observed in  $B_{2g}$  channel was interpreted as a pair-breaking peak originated from the electron pockets around  $M$  point [12]. While  $\text{Fe}_{1+y}\text{Te}_{0.6}\text{Se}_{0.4}$  and  $\text{Ba}(\text{Fe}_{0.939}\text{Co}_{0.061})_2\text{As}_2$  share similar FS topology, these differences suggest that the Raman vertex in the  $B_{2g}$  channel for multi-band FeSCs is rather complex.

*Phonon self-energy effects* – The frequency and line-width for the  $B_{1g}(\text{Fe})$  phonon are presented in Fig. 4(b-c). Above  $T_c$ , the  $B_{1g}(\text{Fe})$  phonon shows a conventional temperature dependence: hardening and sharpening upon cooling following the anharmonic phonon decay model [40–42]. Below  $T_c$ , in contrast to the  $A_{1g}(\text{Te/Se})$  phonon which barely changes upon cooling across  $T_c$  [inset of Fig. 4(a)], the  $B_{1g}(\text{Fe})$  mode shows abnormal behavior in the SC state. The mode's energy and line-width show additional hardening and sharpening in the SC state [Fig. 4(a)].

The  $B_{1g}(\text{Fe})$  phonon energy is around  $26 \text{ meV}$ . It is much larger than the twice of the maximum gap  $2\Delta_3 = 8.4 \text{ meV}$  in  $\text{Fe}_{1+y}\text{Te}_{0.6}\text{Se}_{0.4}$  [32]. For a phonon with  $\omega > 2\Delta$ , such hardening upon entering into SC state was also reported for  $\text{MgB}_2$  [43], for cuprate superconductors [44–49], and for FeSCs [19–21]. The effects were explained within the Zeyher-Zwickyagl's model [50] as a consequence of electron-phonon coupling. When the SC gap opens below  $T_c$ , the electronic density-of-states around the Fermi level is reorganized and pushed above the  $2\Delta$  energies to the proximity of the phonon energy, then the real part of the phonon self-energy shifts to higher energies due to the renormalization by electron-phonon coupling.

However, the Zeyher-Zwickyagl's model predicts that the line-width for a phonon with  $\omega > 2\Delta$  should be broadened upon entering the SC state as the phonon has additional decay channels. To the contrary, the line-width for the  $B_{1g}(\text{Fe})$  phonon for  $\text{Fe}_{1+y}\text{Te}_{0.6}\text{Se}_{0.4}$  further decreases in the SC state. Similar sharpening of the  $B_{1g}(\text{Fe})$  phonon in the SC state was also observed for  $\text{NaFe}_{0.97}\text{Co}_{0.03}\text{As}$  [20],  $\text{Ba}_{0.72}\text{K}_{0.28}\text{Fe}_2\text{As}_2$  [19] and  $\text{Sr}_{0.85}\text{K}_{0.15}\text{Fe}_2\text{As}_2$  [19].

To quantitatively estimate the SC induced self-energy effects and the electron-phonon coupling constant, we use the following model to fit the  $B_{1g}(\text{Fe})$  phonon:  $\chi''_{ph}(\omega) \propto 4\omega_0^2 \Sigma'' [(\omega^2 - \omega_0^2 - 2\omega_0 \Sigma')^2 + 4(\omega_0 \Sigma'')^2]^{-1}$ , where  $\omega_0$  is the bare phonon frequency and  $\Sigma = \Sigma' + i\Sigma''$  is complex phonon self-energy [50]. The phonon appears at  $\omega_{ph} = \sqrt{\omega_0^2 + 2\omega_0 \Sigma'}$  if  $\Sigma''$  is small. The fitting results are presented in Fig. 4(b-c) [42].

We compute the electron-phonon coupling constant  $\lambda_{B_{1g}}$  for the  $B_{1g}(\text{Fe})$  phonon at  $\Gamma$  point [51]:  $\lambda = -\kappa \sin u / u$ , where  $\kappa = [(\Sigma'(5 \text{ K}) - \Sigma'(15 \text{ K})) - i(\Sigma''(5 \text{ K}) - \Sigma''(15 \text{ K}))] / \omega_{ph}(15 \text{ K})$  and  $u \equiv \pi + 2i \cosh^{-1}[\omega_{ph}(15 \text{ K}) / 2\Delta]$ . With  $2\Delta = 45 \text{ cm}^{-1}$  obtained

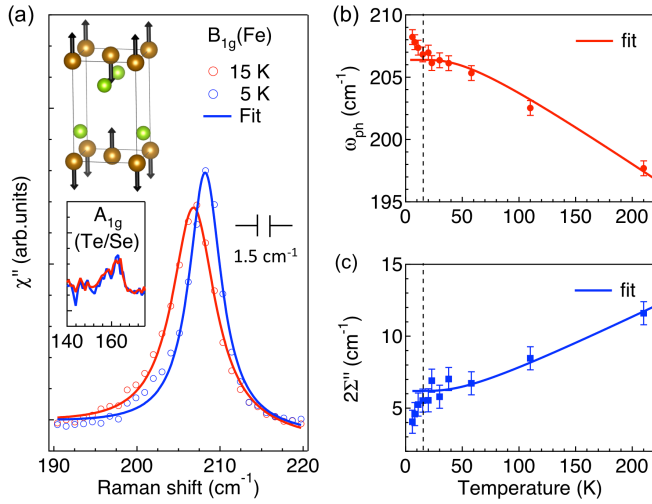


FIG. 4. (a)  $B_{1g}(\text{Fe})$  phonon for  $\text{Fe}_{1+y}\text{Te}_{0.6}\text{Se}_{0.4}$  at 15 K and 5 K in  $X'Y'$  scattering geometry. The top inset of (a) illustrates the atomic displacement of  $B_{1g}(\text{Fe})$  phonon. The bottom inset of (a) shows the  $A_{1g}(\text{Te/Se})$  phonon at 25 K and 5 K in  $XX$  scattering geometry. (b)-(c) T-dependence of the  $B_{1g}(\text{Fe})$  phonon energy  $\omega_{ph}$  and line-width  $2\Sigma''$ .  $\Sigma''$  has been corrected for the instrumental resolution. The solid lines in (b) and (c) represent the fitting of the normal state phonon by anharmonic decay model [42]. The dashed vertical lines in (b) and (c) represent  $T_c$ .

from the pair-breaking peak energy in the  $B_{2g}$  channel, we derive a weak electron-phonon coupling constant  $\lambda_{B_{1g}}^\Gamma \approx 0.026$ . Since the  $A_{1g}(\text{Te/Se})$  phonon shows negligible SC-induced self-energy effect [inset of Fig. 4(a)],  $B_{1g}(\text{Fe})$  phonon is the only phonon that shows such an

effect. Therefore, we can use the  $\lambda_{B_{1g}}^\Gamma$  as an approximation for the averaged electron-phonon coupling constant  $\lambda^\Gamma$  at BZ zone center [21].

By comparison, a much larger electron-phonon coupling constant  $\lambda^\Gamma \approx 0.3$  was reported for a conventional phonon-mediated superconductor  $\text{MgB}_2$  with  $T_c = 39$  K [43]. Furthermore, for  $\text{V}_3\text{Ga}$ , an  $s$ -wave superconductor with a similar  $T_c = 14.2$  K, the electron-phonon coupling constant was estimated to be  $\lambda \approx 0.9$  by optical measurements [52]. Therefore, the electron-phonon coupling constant  $\lambda^\Gamma \approx 0.026$  is clearly insufficient to cause  $T_c = 14$  K superconductivity in  $\text{Fe}_{1+y}\text{Te}_{0.6}\text{Se}_{0.4}$ .

**Conclusions** – In summary, we present polarization-resolved Raman spectroscopic study of single crystal  $\text{Fe}_{1+y}\text{Te}_{0.6}\text{Se}_{0.4}$  superconductor with  $T_c = 14$  K.

In the SC state, we observe a distinct pair-breaking peak at  $45 \text{ cm}^{-1}$  ( $2\Delta = 5.6 \text{ meV}$ ) in the  $B_{2g}$  channel corresponding to the twice of the gap energy (3 meV) on the hole-like FS pocket with  $d_{xz}/d_{yz}$  character around  $\Gamma$  point reported by ARPES measurements.

We analyze the superconductivity induced phonon self-energy effects for the  $B_{1g}(\text{Fe})$  phonon and compute the electron-phonon coupling constant  $\lambda^\Gamma \approx 0.026$ , which is small for  $\text{Fe}_{1+y}\text{Te}_{0.6}\text{Se}_{0.4}$  with  $T_c = 14$  K.

## ACKNOWLEDGMENTS

We thank L.Y. Kong and J.X. Yin for useful discussions. The spectroscopic work at Rutgers (SW, AL and GB) was supported by NSF Grant No. DMR-1709161. Crystal growth and characterization at Technion-Israel Institute of Technology (AA, IF and AK) were supported by Israel Science Foundation grant no: 320/17.

- 
- [1] Y. Kamihara, T. Watanabe, M. Hirano, and H. Hosono, “Iron-based layered superconductor  $\text{LaO}_{1-x}\text{F}_x\text{FeAs}$  ( $x = 0.05 - 0.12$ ) with  $T_c = 26$  K,” *J. Am. Chem. Soc.* **130**, 3296 (2008).
  - [2] J. Paglione and R. L. Greene, “High-temperature superconductivity in iron-based materials,” *Nat. Phys.* **6**, 645–658 (2010).
  - [3] F. Wang and D.-H. Lee, “The electron-pairing mechanism of iron-based superconductors,” *Science* **332**, 200–204 (2011).
  - [4] R. M. Fernandes and A. V. Chubukov, “Low-energy microscopic models for iron-based superconductors: a review,” *Rep. Prog. Phys.* **80**, 014503 (2016).
  - [5] P. J. Hirschfeld, “Using gap symmetry and structure to reveal the pairing mechanism in Fe-based superconductors,” *C. R. Physique* **17**, 197 – 231 (2016).
  - [6] P. C. Dai, “Antiferromagnetic order and spin dynamics in iron-based superconductors,” *Rev. Mod. Phys.* **87**, 855 (2015).
  - [7] Q. M. Si, R. Yu, and E. Abrahams, “High-temperature superconductivity in iron pnictides and chalcogenides,” *Nat. Rev. Mater.* **1**, 16017 (2016).
  - [8] P. Coleman, Y. Komijani, and E. Knig, “The triplet resonating valence bond state and superconductivity in hund’s metals,” *arXiv:1910.03168* (2019).
  - [9] P. Richard, T. Qian, and H. Ding, “ARPES measurements of the superconducting gap of Fe-based superconductors and their implications to the pairing mechanism,” *J. Phys. Condens. Matter* **27**, 293203 (2015).
  - [10] M. H. Fang, H. M. Pham, B. Qian, T. J. Liu, E. K. Vehstedt, Y. Liu, L. Spinu, and Z. Q. Mao, “Superconductivity close to magnetic instability in  $\text{Fe}(\text{Se}_{1-x}\text{Te}_x)_{0.82}$ ,” *Phys. Rev. B* **78**, 224503 (2008).
  - [11] Whether or not the  $d_{xy}$  character hole band crosses the  $E_F$  remains under debate [32, 39]. Thus, we use a dashed circle to represent the outer FS pocket with  $d_{xy}$  character around  $\Gamma$ . The middle solid circle represents the hole-like FS pocket with  $d_{xz}/d_{yz}$  character around the  $\Gamma$  point. The inner dashed circle represents the FS for topological surface band [33]. The ellipses represent the electron-like FS pockets with  $d_{xz}/d_{yz}$  character around the  $M$  point.
  - [12] B. Muschler, W. Prestel, R. Hackl, T. P. Devereaux, J. G. Analytis, Jiun-Haw Chu, and I. R. Fisher, “Band- and momentum-dependent electron dynamics in super-



- conducting  $\text{Ba}(\text{Fe}_{1-x}\text{Co}_x)_2\text{As}_2$  as seen via electronic Raman scattering,” *Phys. Rev. B* **80**, 180510 (2009).
- [13] L. Chauvière, Y. Gallais, M. Cazayous, M. A. Méasson, A. Sacuto, D. Colson, and A. Forget, “Impact of the spin-density-wave order on the superconducting gap of  $\text{Ba}(\text{Fe}_{1-x}\text{Co}_x)_2\text{As}_2$ ,” *Phys. Rev. B* **82**, 180521 (2010).
- [14] P. Massat, D. Farina, I. Paul, S. Karlsson, P. Strobel, P. Toulemonde, M.-A. Méasson, M. Cazayous, A. Sacuto, S. Kasahara, Y. Shibauchi, T. and Matsuda, and Y. Gallais, “Charge-induced nematicity in  $\text{FeSe}$ ,” *Proc. Natl. Acad. Sci. U.S.A.* **113**, 9177–9181 (2016).
- [15] S. Sugai, Y. Mizuno, K. Kiho, M. Nakajima, C. H. Lee, A. Iyo, H. Eisaki, and S. Uchida, “Pairing symmetry of the multiorbital pnictide superconductor  $\text{BaFe}_{1.84}\text{Co}_{0.16}\text{As}_2$  from Raman scattering,” *Phys. Rev. B* **82**, 140504 (2010).
- [16] T. Böhm, A. F. Kemper, B. Moritz, F. Kretzschmar, B. Muschler, H.-M. Eiter, R. Hackl, T. P. Devereaux, D. J. Scalapino, and Hai-Hu Wen, “Balancing act: Evidence for a strong subdominant  $d$ -wave pairing channel in  $\text{Ba}_{0.6}\text{K}_{0.4}\text{Fe}_2\text{As}_2$ ,” *Phys. Rev. X* **4**, 041046 (2014).
- [17] S.-F. Wu, P. Richard, H. Ding, H.-H. Wen, Guotai Tan, Meng Wang, Chenglin Zhang, Pengcheng Dai, and G. Blumberg, “Superconductivity and electronic fluctuations in  $\text{Ba}_{1-x}\text{K}_x\text{Fe}_2\text{As}_2$  studied by Raman scattering,” *Phys. Rev. B* **95**, 085125 (2017).
- [18] V. K. Thorsmølle, M. Khodas, Z. P. Yin, Chenglin Zhang, S. V. Carr, Pengcheng Dai, and G. Blumberg, “Critical quadrupole fluctuations and collective modes in iron pnictide superconductors,” *Phys. Rev. B* **93**, 054515 (2016).
- [19] K.-Y. Choi, P. Lemmens, I. Eremin, G. Zwicknagl, H. Berger, G. L. Sun, D. L. Sun, and C. T. Lin, “Self-energy effects and electron-phonon coupling in  $\text{FeAs}$  superconductors,” *J. Phys. Condens. Matter* **22**, 115802 (2010).
- [20] Y. J. Um, Yunkyu Bang, B. H. Min, Y. S. Kwon, and M. Le Tacon, “Superconductivity-induced phonon renormalization on  $\text{NaFe}_{1-x}\text{Co}_x\text{As}$ ,” *Phys. Rev. B* **89**, 184510 (2014).
- [21] W.-L. Zhang, W. R. Meier, T. Kong, P. C. Canfield, and G. Blumberg, “High- $T_c$  superconductivity in  $\text{CaKFe}_4\text{As}_4$  in absence of nematic fluctuations,” *Phys. Rev. B* **98**, 140501 (2018).
- [22] T. L. Xia, D. Hou, S. C. Zhao, A. M. Zhang, G. F. Chen, J. L. Luo, N. L. Wang, J. H. Wei, Z. Y. Lu, and Q. M. Zhang, “Raman phonons of  $\alpha$ - $\text{FeTe}$  and  $\text{Fe}_{1.03}\text{Se}_{0.3}\text{Te}_{0.7}$  single crystals,” *Phys. Rev. B* **79**, 140510 (2009).
- [23] V. Gnezdilov, Yu. Pashkevich, P. Lemmens, A. Gusev, K. Lamonova, T. Shevtsova, I. Vitebskiy, O. Afanasiev, S. Gnatchenko, V. Tsurkan, J. Deisenhofer, and A. Loidl, “Anomalous optical phonons in  $\text{FeTe}$  chalcogenides: Spin state, magnetic order and lattice anharmonicity,” *Phys. Rev. B* **83**, 245127 (2011).
- [24] Y. J. Um, A. Subedi, P. Toulemonde, A. Y. Ganin, L. Boeri, M. Rahlenbeck, Y. Liu, C. T. Lin, S. J. E. Carlsson, A. Sulpice, M. J. Rosseinsky, B. Keimer, and M. Le Tacon, “Anomalous dependence of  $c$ -axis polarized  $\text{Fe } B_{1g}$  phonon mode with  $\text{Fe}$  and  $\text{Se}$  concentrations in  $\text{Fe}_{1+y}\text{Te}_{1-x}\text{Se}_x$ ,” *Phys. Rev. B* **85**, 064519 (2012).
- [25] K. Okazaki, S. Sugai, S. Niitaka, and H. Takagi, “Phonon, two-magnon, and electronic Raman scattering of  $\text{Fe}_{1+y}\text{Te}_{1-x}\text{Se}_x$ ,” *Phys. Rev. B* **83**, 035103 (2011).
- [26] S. Rinott, K. B. Chashka, A. Ribak, Emile D. L. Rienks, A. Taleb-Ibrahimi, P. Le Fevre, F. Bertran, M. Randeria, and A. Kanigel, “Tuning across the BCS-BEC crossover in the multiband superconductor  $\text{Fe}_{1+y}\text{Se}_x\text{Te}_{1-x}$ : An angle-resolved photoemission study,” *Sci. Adv.* **3**, e1602372 (2017).
- [27] F. Kretzschmar, T. Böhm, U. Karahasanovic, B. Muschler, A. Baum, D. Jost, J. Schmalian, S. Caprara, M. Grilli, C. Di Castro, J. G. Analytis, J.-H. Chu, I. R. Fisher, and R. Hackl, “Critical spin fluctuations and the origin of nematic order in  $\text{Ba}(\text{Fe}_{1-x}\text{Co}_x)_2\text{As}_2$ ,” *Nat. Phys.* **12**, 560 (2016).
- [28] W.-L. Zhang, S.-F. Wu, S. Kasahara, T. Shibauchi, Y. Matsuda, G. Blumberg, “Stripe quadrupole order in the nematic phase of  $\text{FeSe}_{1-x}\text{S}_x$ ,” [arXiv:1710.09892](https://arxiv.org/abs/1710.09892) (2017).
- [29] T. P. Devereaux and R. Hackl, “Inelastic light scattering from correlated electrons,” *Rev. Mod. Phys.* **79**, 175–233 (2007).
- [30] Y. Gallais, R. M. Fernandes, I. Paul, L. Chauvière, Y.-X. Yang, M.-A. Méasson, M. Cazayous, A. Sacuto, D. Colson, and A. Forget, “Observation of incipient charge nematicity in  $\text{Ba}(\text{Fe}_{1-x}\text{Co}_x)_2\text{As}_2$ ,” *Phys. Rev. Lett.* **111**, 267001 (2013).
- [31] The phonon frequencies and the line-widths for  $A_{1g}(\text{Te/Se})$  and  $B_{1g}(\text{Fe})$  phonons are derived by fitting the spectra in the  $c(aa)\bar{c}$  scattering geometry at 5 K shown in Fig. 4 of the Ref. [25] by Lorentzian functions with a linear background. Since the instrumental resolution is not given in Ref. [25], the line-widths are not corrected for the instrumental broadening.
- [32] H. Miao, P. Richard, Y. Tanaka, K. Nakayama, T. Qian, K. Umezawa, T. Sato, Y.-M. Xu, Y. B. Shi, N. Xu, X.-P. Wang, P. Zhang, H.-B. Yang, Z.-J. Xu, J. S. Wen, G.-D. Gu, X. Dai, J.-P. Hu, T. Takahashi, and H. Ding, “Isotropic superconducting gaps with enhanced pairing on electron Fermi surfaces in  $\text{FeTe}_{0.55}\text{Se}_{0.45}$ ,” *Phys. Rev. B* **85**, 094506 (2012).
- [33] P. Zhang, K. Yaji, T. Hashimoto, Y. Ota, T. Kondo, K. Okazaki, Z. J. Wang, J. S. Wen, G. D. Gu, H. Ding, and S. Shin, “Observation of topological superconductivity on the surface of an iron-based superconductor,” *Science* **360**, 182–186 (2018).
- [34] J.-X. Yin, Zheng Wu, J.-H. Wang, Z.-Y. Ye, Jing Gong, X.-Y. Hou, Lei Shan, Ang Li, X.-J. Liang, X.-X. Wu, Jian Li, C.-S. Ting, Z.-Q. Wang, J.-P. Hu, P.-H. Hor, H. Ding, and S. H. Pan, “Observation of a robust zero-energy bound state in iron-based superconductor  $\text{Fe}(\text{Te,Se})$ ,” *Nat. Phys.* **11**, 543 (2015).
- [35] C. C. Homes, A. Akrap, J. S. Wen, Z. J. Xu, Z. W. Lin, Q. Li, and G. D. Gu, “Electronic correlations and unusual superconducting response in the optical properties of the iron chalcogenide  $\text{FeTe}_{0.55}\text{Se}_{0.45}$ ,” *Phys. Rev. B* **81**, 180508 (2010).
- [36] R. Escudero and R. E. López-Romero, “The energy gap of the compound  $\text{FeSe}_{0.5}\text{Te}_{0.5}$  determined by specific heat and point contact spectroscopy,” *Solid State Commun.* **220**, 21–24 (2015).
- [37] Y. M. Qiu, W. Bao, Y. Zhao, C. Broholm, V. Stanev, Z. Tesanovic, Y. C. Gasparovic, S. Chang, Jin Hu, Bin Qian, M. H. Fang, and Z. Q. Mao, “Spin gap and resonance at the nesting wave vector in superconducting  $\text{FeSe}_{0.4}\text{Te}_{0.6}$ ,” *Phys. Rev. Lett.* **103**, 067008 (2009).
- [38] T. Hanaguri, S. Niitaka, K. Kuroki, and H. Takagi, “Unconventional  $s$ -wave superconductivity in  $\text{Fe}(\text{Se,Te})$ ,” *Science* **328**, 474–476 (2010).

- [39] P. Zhang, Z. J. Wang, X. X. Wu, K. Yaji, Y. Ishida, Y. Kohama, G. Y. Dai, Y. Sun, C. Bareille, K. Kuroda, T. Kondo, K. Okazaki, K. Kindo, X. C. Wang, C. Q. Jin, J. P. Hu, R. Thomale, K. Sumida, S. L. Wu, K. Miyamoto, T. Okuda, H. Ding, G. D. Gu, T. Tamegai, T. Kawakami, M. Sato, and S. Shin, “Multiple topological states in iron-based superconductors,” *Nat. Phys.* **15**, 41–47 (2019).
- [40] P. G. Klemens, “Anharmonic decay of optical phonons,” *Phys. Rev.* **148**, 845 (1966).
- [41] J. Menéndez and M. Cardona, “Temperature dependence of the first-order Raman scattering by phonons in Si, Ge, and  $\alpha$ -Sn: Anharmonic effects,” *Phys. Rev. B* **29**, 2051 (1984).
- [42] Above  $T_c$ , the temperature dependence of the frequency and line-width for the  $B_{1g}(\text{Fe})$  phonon can be fitted by  $\omega_{ph}(T) = \omega_0 - C(1 + 2/(e^{\hbar\omega_0/2k_B T} - 1))$ ,  $\Gamma_{ph}(T) = \Gamma_0 + \Gamma_1(1 + 2/e^{\hbar\omega_0/2k_B T} - 1)$ . The fitting parameters for  $\omega_0$ ,  $C$ ,  $\Gamma_0$ ,  $\Gamma_1$  are  $211.1 \text{ cm}^{-1}$ ,  $4.8 \text{ cm}^{-1}$ ,  $3.2 \text{ cm}^{-1}$  and  $2.9 \text{ cm}^{-1}$ , respectively.
- [43] A. Mialitsin, B. S. Dennis, N. D. Zhigadlo, J. Karpinski, and G. Blumberg, “Anharmonicity and self-energy effects of the  $E_{2g}$  phonon in  $\text{MgB}_2$ ,” *Phys. Rev. B* **75**, 020509 (2007).
- [44] S. L. Cooper, M. V. Klein, B. G. Pazol, J. P. Rice, and D. M. Ginsberg, “Raman scattering from superconducting gap excitations in single-crystal  $\text{YBa}_2\text{Cu}_3\text{O}_{7-\delta}$ ,” *Phys. Rev. B* **37**, 5920–5923 (1988).
- [45] C. Thomsen, M. Cardona, B. Gegenheimer, R. Liu, and A. Simon, “Untwinned single crystals of  $\text{YBa}_2\text{Cu}_3\text{O}_{7-\delta}$ : An optical investigation of the  $a - b$  anisotropy,” *Phys. Rev. B* **37**, 9860–9863 (1988).
- [46] B. Friedl, C. Thomsen, and M. Cardona, “Determination of the superconducting gap in  $\text{RBa}_2\text{Cu}_3\text{O}_{7-\delta}$ ,” *Phys. Rev. Lett.* **65**, 915–918 (1990).
- [47] K. F. McCarty, H. B. Radousky, J. Z. Liu, and R. N. Shelton, “Temperature dependence of the linewidths of the Raman-active phonons of  $\text{YBa}_2\text{Cu}_3\text{O}_7$ : Evidence for a superconducting gap between 440 and  $500 \text{ cm}^{-1}$ ,” *Phys. Rev. B* **43**, 13751–13754 (1991).
- [48] G. Blumberg, M. V. Klein, L. Börjesson, R. Liang, and W. N. Hardy, “Investigation of the temperature dependence of electron and phonon Raman scattering in single crystal  $\text{YBa}_2\text{Cu}_3\text{O}_{6.952}$ ,” *J. Supercond* **7**, 445 (1994).
- [49] C. Thomsen and M. Cardona, “Raman scattering in high- $T_c$  superconductors,” in *Physical Properties of High Temperature Superconductors I*, Chap. 8, pp. 409–507.
- [50] R. Zeyher and G. Zwirgagl, “Superconductivity-induced phonon self-energy effects in hightcsuperconductors,” *Zeitschrift für Physik B Condensed Matter* **78**, 175–190 (1990).
- [51] C. O. Rodriguez, A. I. Liechtenstein, I. I. Mazin, O. Jepsen, O. K. Andersen, and M. Methfessel, “Optical near-zone-center phonons and their interaction with electrons in  $\text{YBa}_2\text{Cu}_3\text{O}_7$ : Results of the local-density approximation,” *Phys. Rev. B* **42**, 2692–2695 (1990).
- [52] E. G. Maksimov and G. P. Motulevich, “Determination of the electron-phonon coupling constant from optical measurements,” *Sov. Phys.-JETP* **34**, 219–221 (1972).